Three-dimensional crystalline ion beams

U. Schramm,* T. Schätz, and D. Habs

Ludwig-Maximilians-Universität München, Sektion Physik, D-85748 Garching, Germany
(Received 9 October 2001; published 10 September 2002)

We report on the experimental realization of two- and three-dimensional crystalline ion beams in the rf quadrupole storage ring PALLAS (LMU, Munich). At a beam energy around 1 eV the phase transition to the Coulomb ordered state is identified by a sudden decrease of the spatial width and of the velocity spread of the beam. The focusing conditions required to attain crystalline beams up to structures of helices surrounding a string are systematically investigated and related to the situation in typical heavy ion storage rings.

I. INTRODUCTION

The phase transition [1–3] of an emittance dominated *gaseous* ion beam to a one-dimensional Coulomb ordered *crystalline* beam, a string of ions, was recently realized at the rf quadrupole storage ring PALLAS at a beam energy of about 1 eV [4–6]. In the crystalline state, the state of ultimate brilliance, the ions reside on well-defined lattice positions. This order implies that dissipative close Coulomb collisions between constituent ions are suppressed. As a consequence, the beams were observed to decouple from their environment and to exhibit negligible emittance growth.

The realization of three-dimensional crystalline beams, where a larger number of ions are expected to arrange themselves into helical structures [7–9], should open perspectives beyond standard accelerator physics concerning the attainable phase space density of ion beams. Of particular interest is the complex interplay of three-dimensional crystalline beams with the periodic focusing and bending elements of a storage ring. In contrast to the latter one-dimensional ion strings, these beams extend into the transverse plane. They experience an increased interaction with the alternating confining fields as well as they have to withstand bending shear. The maintenance of crystalline beams is therefore expected to impose severe constraints to the periodic storage ring lattice [10–13], which can be studied in the rf quadrupole storage ring PALLAS.

II. THE rf QUADRUPOLE STORAGE RING

The low-energy ion storage ring PALLAS, sketched in Fig. 1, basically resembles a circular rf quadrupole ion guide [4–6,8]. Between the quadrupole ring electrodes typical rf voltages of $U_{rf} \simeq 100–400$ V are applied at a fixed frequency of $\Omega = 2\pi \times 6.3$ MHz. Inside the rf quadrupole structure an ion beam experiences an oscillating transverse force with a period length of $L = 2\pi v/\Omega$, where v denotes the nominal beam velocity. This technique of alternating focusing and defocusing (known as *strong focusing* [14] in conventional accelerators) results in the transverse confinement of the ion

beam on a closed orbit with a circumference of $C = 361$ mm in the case of the storage ring PALLAS. Close to the center of the quadrupole structure the net restoring force can be approximated by a harmonic pseudopotential $\Psi(r) = (qU_{rf}/8)(r/r_0)^2$ [15]. It is usually characterized by the stability parameter $q = 2eU_{rf}/(m\Omega^2 r_0^2) \simeq 0.08–0.32$, where e and m stand for the charge and mass of the ^{24}Mg$^+$ ions and $r_0 = 2.5$ mm for the aperture radius of the quadrupole structure. The corresponding single-particle secular frequency $\omega_{sec} = q\Omega/\sqrt{8}$ varies between $\omega_{sec} \simeq 2\pi \times (200–700)$ kHz. This transverse secular motion is equivalent to the betatron motion in a conventional storage ring, where the particles oscillate in the fields of alternating focusing and defocusing (quadrupole) magnets [14], and where the overall focusing strength is given by the corresponding number of oscillations per round-trip, the betatron *tune* $Q = \omega_{sec}/\omega_{rev}$. In the rf quadrupole storage ring the tune $Q = (\omega_{sec}/2\pi)C/v$ becomes velocity dependent. For a typical beam velocity of $v = 2800$ m/s, which corresponds to a beam energy of ≈ 1 eV, it amounts to $Q \simeq 25–90$. The number of identical focusing sections in the storage ring, the *periodicity P* $= C/L$, is given by the ratio of the driving rf frequency Ω to the revolution frequency $P = \Omega/\omega_{rev} \approx 800$. The motion of an ion beam in the storage ring PALLAS can thus be fully described in the usual storage ring terminology [16]. Moreover, the focusing conditions can be systematically varied over a wide range.
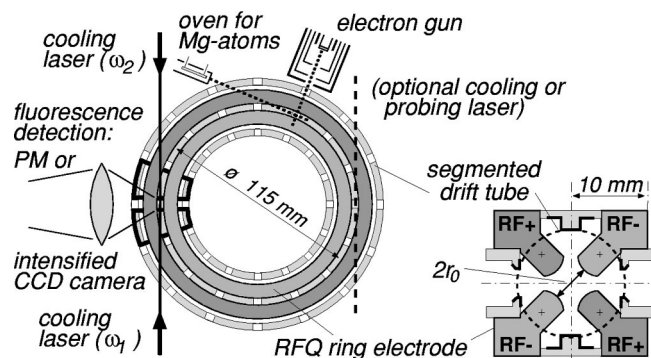

FIG. 1. Axial and radial cut through the rf quadrupole storage ring PALLAS. Ions are confined on a circular orbit, enclosed by the quadrupole ring electrodes. Sixteen segmented drift tubes enable the manipulation of ions along the direction of the orbit.

*Email address: ulrich.schramm@physik.uni-muenchen.de; URL: http://www.ha.physik.uni-muenchen.de/uschramm/
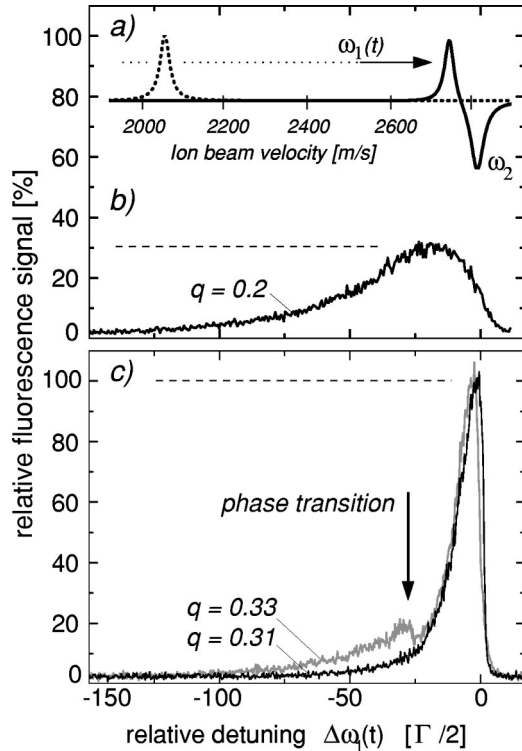
FIG. 2. Fluorescence signal of the ion beam as a function of the frequency of the scanning copropagating laser beam (scan time 4 s). The frequency is given in terms of the relative detuning $\Delta\omega_1(t)$ from the resonance at $v = 2800$ m/s and in units of half the natural transition linewidth $\Gamma = 2\pi \times 42.7$ MHz. The corresponding laser forces are sketched in (a) as a function of the ion velocity. In (b) the broad fluorescence signal of a noncrystalline beam is depicted, whereas in (c) the pronounced discontinuity of the gray curve and the sharp drop-off is characteristic of the phase transition to the ordered beam. With slightly reduced rf heating the phase transition sets in earlier. The characteristic "dip" cannot be resolved anymore (black curve) and the fluorescence signal drops off even later. (Reprinted from [4] with permission from Macmillan Magazines, Ltd.)

To load the ring with ions, a weak collimated beam of ^{24}Mg atoms is ionized inside the trapping volume by a focused electron beam. Stored ions are immediately guided into the interaction region, where two counterpropagating laser beams tangentially cover about 1% of the ring circumference, as sketched in Fig. 1. Both laser beams address the closed $3s^2S_{1/2}$-$3p^2P_{3/2}$ transition of the ^{24}Mg$^+$ ion at a wavelength of 280 nm. The ions are Doppler laser cooled [17] to form a stationary cloud at zero center-of-mass velocity $v = 0$. The resonance fluorescence is recorded with a fast photomultiplier and imaged with an intensified charge coupled device camera with a typical spatial resolution of 4.5 μm.

After the accumulation of ions at a rate of roughly 1000 s^{-1}, the resonant light pressure of the copropagating laser beam is used to accelerate the cold ion ensemble [4–6]. The frequency of the copropagating laser beam ω_1 is continuously increased as sketched in Fig. 2(a) until the accelerated ions come into resonance with the decelerating counterpropagating laser beam. Its fixed frequency ω_2 is set to

define the nominal beam velocity of $v = 2800$ m/s. The longitudinal velocity spread of the ion beam is efficiently reduced due to the dispersive character of the combined laser force. The damping of the transverse ion motion perpendicular to the laser beams is provided indirectly by the interparticle Coulomb interaction [18] and by a slight tilt of the laser beams with respect to the ion beam [19].

The typical behavior of a cold ion beam, which contains $N = 18\,000$ particles, is shown in Fig. 2(b) [4,6]. The fluorescence rate increases as the frequency detuning of the copropagating laser beam is decreased. Close to the resonance the forces start to compensate and the rate drops off again. At the end of the frequency scan the laser is reset to a frequency that corresponds to a velocity change of about -1000 m/s, and the cycle restarts.

III. CRYSTALLINE ION BEAMS

An increase of the confining potential drastically changes the behavior, as demonstrated in Fig. 2(c). At first (gray curve), the fluorescence signal follows the previous curve. Then, as marked by the arrow, it decreases abruptly and subsequently rises to a sharp asymmetric peak. This signature of a dip in the fluorescence signal was originally observed in ion traps for small ion ensembles [20]. It was interpreted as a result of the competition between laser cooling and rf heating, which first grows when the phase space density increases and then abruptly vanishes when the ion ensemble crystallizes [21,22]. Thus, the observation of this signature in the fluorescence signal of a laser-cooled beam in the storage ring PALLAS served as a first indication of the phase transition to a crystalline beam [4,6]. With slightly reduced confinement and thus with reduced rf heating the phase transition sets in earlier and the dip cannot be resolved any more (black curve). A comparison of Figs. 2(b) and 2(c) shows that, in the storage ring PALLAS, the peak rate emitted by a noncrystalline ensemble amounts to about 30% of the peak rate of the corresponding crystalline ensemble.

The structure of crystalline beams was studied in molecular dynamics (MD) simulations [7] and observed in experiments with elongated ion crystals in ring-shaped [8] and linear [9] rf quadrupole traps. It is believed to uniquely depend on the dimensionless *linear density* $\lambda = (N/C)a$. The linear density is expressed in terms of the Wigner-Seitz radius $a = \{[1/(4\pi\varepsilon_0)]3e^2/(2m\omega_{sec}^2)\}^{1/3} \simeq 10$ μm to account for the dominant influence of the confining potential on the structure of the ion crystal, as described below. The number of particles in the crystalline beam N can be determined from the peak fluorescence rate of the beam which is recorded when the accelerating laser is repeatedly scanned [Fig. 2(c)]. The accuracy of this method amounts to about 10% [23].

The linear density of the crystalline beam presented in Fig. 2(c) amounts to $\lambda = 0.4$ ($N = 18\,000$). This value corresponds to the formation of a linear string of ions ($\lambda < 0.71$) along the orbit. As reported earlier [4,6], the phase transition to this *one-dimensional* (1D) crystalline beam is accompanied by a sudden drop of the spatial transverse beam profile. After the phase transition the beam profile resembles that of a stationary string of ions in agreement with the above clas-

sification ($\lambda < 0.71$). The longitudinal temperature in the co-moving reference frame $T_\parallel$ was measured to be below 3 mK. The corresponding *plasma parameter* $\Gamma_p = [1/(4\pi\varepsilon_0)] \times (e^2/a)[1/(kT_\parallel)]$, which describes the inter-ion coupling strength, therefore amounts to $\Gamma_p > 500$. This value clearly exceeds the threshold of $\Gamma_p^{(3D)} \simeq 180$, postulated for the formation of infinite three-dimensional ion crystals [24–26].

In contrast to stationary ion crystals where the fluorescence image of individual ions can be resolved [4,8,9], the determination of 2D and 3D crystalline beams has to rely on indirect methods. Still, the evolution of a 1D string of ions ($\lambda < 0.71$) into a 2D zigzag band ($0.71 < \lambda < 0.96$) [7] can be unambiguously followed, as discussed in the following.

A. Two-dimensional crystalline beams

In Fig. 3(a), the image of a crystalline beam ($N = 26\,500$) is presented, which corresponds to the configuration of a linear string of ions. As its linear density ($\lambda = 0.7$) is close to the threshold for the transition from the 1D string to the 2D zigzag configuration, a change of the configuration can be induced by a slight decrease of the confining potential ($q = 0.22 \to 0.20$). This decrease corresponds to an increase of the Wigner-Seitz radius a and thus to an increase in the linear density of $\lambda = 0.70 \to 0.77 > 0.71$. The image of the resulting zigzag structure is presented in Fig. 3(b). In Fig. 3(d), the vertical beam profile is enlarged. Its absolute shape can be reproduced by the composition of two profiles of the corresponding linear string, divided in amplitude by a factor of 2 and displaced vertically by $\Delta = \pm 6\ \mu$m. Furthermore, a similar discontinuity (dip) in the fluorescence signal [Fig. 3(c)] was found when the laser was continuously scanned as in the case of the string. Very close to this threshold a bistable behavior between the two configurations was observed on a time scale of several 100 ms.

The orientation of the zigzag beam was found to be always vertical. For horizontal orientation the mean kinetic energy per ion E_k in the zigzag band amounts to $E_k = m\omega_{rev}^2[(R - \Delta_x)^2 + (R + \Delta_x)^2]/4 = m\omega_{rev}^2(2R^2 + 2\Delta_x^2)/4$. Obviously, the vertical orientation ($\Delta_x = 0$) is energetically favorable and thus minimizes the influence of bending shear.

Compared to the profile of stationary 2D crystals [see [4,8] and the longitudinally blurred image of a long stationary crystal in Fig. 3(e)], the contrast of the beam profile is markedly reduced. This effect is, on the one hand, due to the comparatively low integrated signal rate of the laser-cooled ion beam [27], and, on the other hand, possibly due to local fluctuations of the linear density within the 36-cm-long crystalline beam. It has to be emphasized that the measured profiles of the zigzag beam as well as of the stationary ion crystals do not show the expected sharp cutoff at the edges, but sit on a distinct Gaussian pedestal. This pedestal is attributed to scattering of fluorescence light in the optical imaging system [28] and must not be confused with a real beam halo as discussed later in the text.

B. Three-dimensional crystalline beams

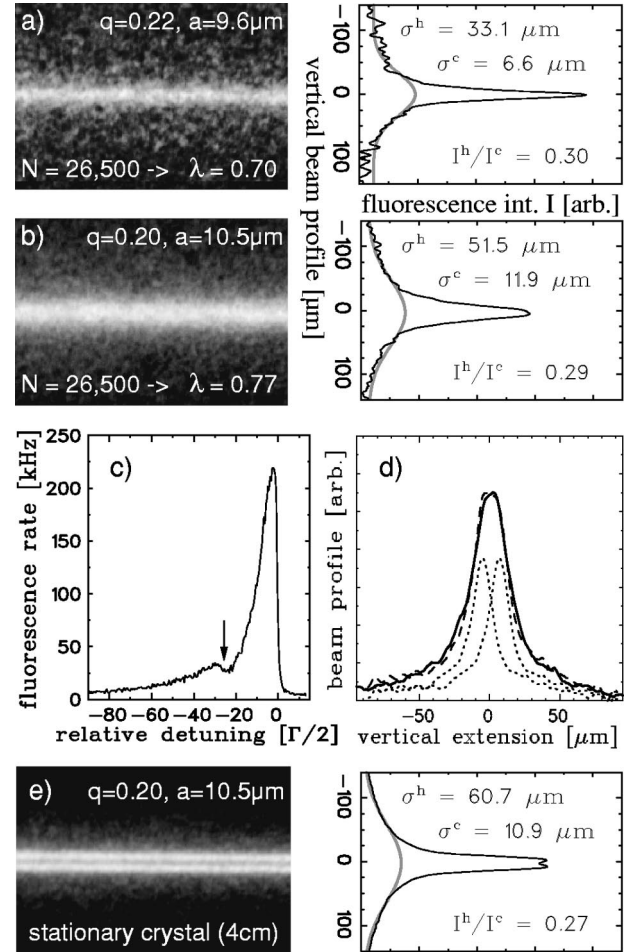Based on the assumption of cylindrical confinement, 3D crystalline beams are expected to exhibit more complex

FIG. 3. The images (a)$\to$(b) show the change in the profile of a crystalline ion beam when its linear density is crossing the threshold value of $\lambda = 0.71$. The string of ions transforms into a zigzag band. In (c), the fluorescence rate emitted by this zigzag beam is depicted as a function of the continuous laser detuning. In (d) its shape (solid line) is compared with a composition (dashed line) of two profiles (dotted lines) of the string halved in amplitude and vertically displaced by $\pm 6\ \mu$m. The profile (e) belongs to a stationary ion crystal (zigzag, ≈ 4 cm long) where the image of individual ions is blurred. For the determination of the width σ^c of stationary ion crystals and of crystalline beams, a Gaussian distribution (width σ^h, amplitude I^h) is fitted to the noticeable pedestal and subtracted [32].

structures [7] at a rather constant average ion density [25]: helices ($0.96 < \lambda < 3.1$), helices surrounding a string ($3.1 < \lambda < 5.7$), and multishell helices ($5.7 < \lambda$). The determination of the state and the structure of a beam relies on a combination of arguments, which is based on the experience with 1D [4,5] and 2D [6] crystalline beams in the storage ring PALLAS: First, and the most obvious when performing the experiment, the phase transition is accompanied by a sudden change of the transverse beam profile and of the shape and the maximum yield of the fluorescence signal when the laser is scanned (compare Fig. 2). Second, the emittance growth of the crystalline beam is drastically reduced compared to noncrystalline beams [4,6]. Without cooling, the beams ($0.2 < \lambda < 1.3$) were observed to remain in the crystalline state for about 1000 revolutions in the storage

ring (≈ 200 ms or $\approx 10^6$ rf cycles) as reported in detail in [29]. This fact demonstrates the suppression of close Coulomb collisions within the beam, which is a strong evidence for Coulomb order [10–12,30]. Third, the beam radii agree with the predicted values [7], which are commonly used to describe the appearance of elongated stationary crystals [4,8,9]. Although, for the third, it could be argued, that the distinction of a crystalline and a cold but fluid beam is hardly possible from the beam radius [25], heating through intrabeam scattering is expected to decrease when the ordering sets in [12,13,30]. Therefore, as this point is reached, and none of the proposed maintenance conditions (see, e.g., [2,11,12,31]) are violated, the ensemble is expected to collapse into the crystalline state.

Typical vertical profiles of stored beams containing $N \approx 80\,000$ ions ($\lambda \approx 2.7$) are presented in Fig. 4. In analogy to the aforementioned generation of 1D and 2D crystalline ion beams, the phase transition from a gaseous beam [Fig. 4(a) and open triangles and circles in the following figures] to a three-dimensional crystalline beam [Fig. 4(b) and filled triangles and circles in the following figures] is accompanied by a sudden reduction of the width of the beam. Simultaneously, the integral fluorescence rate increases by about a factor of 3, as presented for the case of 1D beams (Fig. 2). The transition can be induced by an increase of the transverse confinement which enhances the coupling between the directly cooled longitudinal and the transverse degrees of freedom. In contrast to the behavior of 1D crystalline beams, the profile changes significantly with further rising confining potential [Fig. 4(c) and crossed symbols]. The absolute width of the beam increases by a factor of about 1.5 although its appearance remains similar to that of a crystalline beam. For even higher values of the potential the beam clearly melts (dotted symbols), and the profile cannot be distinguished from the original broad noncrystalline one, presented in Fig. 4(a).

The behavior described in the above example is illustrated in greater detail in Fig. 5, where the measured width σ^c of a series of beams containing different particle numbers is plotted against the applied rf voltage U_{rf}. With the use of the relation $\sigma^c/a \propto \sqrt{\lambda}$ and thus $\sigma^c U_{rf}^{2/3} \propto \sqrt{\lambda}$, which is established for stationary ion crystals [7–9], (solid) contour lines are drawn for the threshold values of constant linear density where a change of the structure of a crystalline beam is expected. In this way, the classification of crystalline beams (filled symbols) only relies on the determination of the width of the beam σ^c and of the rf voltage U_{rf}, both of which are known to be better than $\pm 5\%$ [32].

C. Focusing conditions

We now discuss the conditions for which crystalline beams of different linear density were attainable in the storage ring PALLAS. Crystalline beams were observed to occur only in a specific region in the U_{rf}-σ^c diagram (filled symbols in Fig. 5), which resembles a curved band: with increasing radius of the (3D) crystalline beam the required focusing strength decreases. This band is noticeably narrow compared to the width of the region of stability which was found for

stationary crystals [4,8]. The latter can be found below the dotted line in Fig. 5. This discrepancy might be due to the transient cooling of the ion beam on a fraction of only 1% of the circumference of the storage ring. This cooling scheme allows the accumulation of external perturbations during one round trip. For the periodic transverse modulation of a crystalline beam in the alternating focusing and defocusing fields, Schiffer derived an estimate for the corresponding spread in the transverse ion velocities [11] as a function of the radius of a crystalline beam. It can be related to an apparent temperature T_{app}^f, or an apparent plasma parameter $\Gamma_{app}^f = [1/(4\pi\varepsilon_0)](e^2/a)[1/(kT_{app}^f)]$, respectively. Γ_{app}^f decreases with increasing linear density and focusing strength as

$$\Gamma_{app}^f \propto (1/\lambda)(P/Q)^2 \propto 1/(\sigma^c U^{5/3})^2 \propto 1/(\sqrt{\lambda}\,\omega_{sec})^2. \quad (1)$$

The curvature of the band of stability in Fig. 5 is reproduced by the dashed line surprisingly well. This line follows Eq. (1) for a threshold value of $\Gamma_{app}^f \simeq 180$, which is required for the formation of large 3D ion crystals [24,26]. Yet, it has to be emphasized that this driven periodic transverse motion in the quadrupole potential should not be regarded as random or thermal motion. For stationary crystals [4,33] as well as for crystalline beams [10,13,29] it was shown in simulations as well as in experiments that the energy transfer from the periodic to the random motion is strongly suppressed compared to the noncrystalline ensemble. On the other hand, for beams which are not sufficiently cold (i.e., below the critical plasma parameter of $\Gamma_p^f \simeq 180$ and thus above the dashed line in Fig. 5) the coupling of collective motion into random motion is expected to increase due to intrabeam scattering [12,13,21,30].

For the comparison with synchrotrons, where magnetic focusing is used, Fig. 5 is translated into a λ-Q diagram [Fig. 6(b)]. In this case, the tune $Q = \omega_{sec}/\omega_{rev}$ characterizes the velocity invariant focusing strength. In the complementary Fig. 6(a), the corresponding secular frequency ω_{sec}, which is more appropriate to describe the velocity invariant focusing strength for the case of electric focusing in the rf quadrupole storage ring PALLAS, is depicted. Since, at random, the largest crystalline beams were recorded at lower velocities ($v \simeq 1900$ m/s, compared to 2800 m/s), the corresponding tune $Q \propto U_{rf}/v$ changes less significantly with rising linear density λ than the secular frequency ω_{sec}. The λ-Q as well as the λ-ω_{sec} diagram allows a distinction of the upper and the lower border of the shaded parameter range, where crystalline beams were observable.

As discussed with Fig. 5, the upper focusing limit seems to be related to the periodic transverse modulation of the crystalline beam [dashed line, following Eq. (1)]. Yet, since crystalline beams were observed to survive for $\approx 10^6$ focusing periods in the storage ring PALLAS ($P \simeq 800$) [29] without any cooling, the heating rate of this effect should be small, and the absolute value of this limit is presumed to strongly depend on the specific cooling scheme. Notably, the observed limiting focusing strength lies more than a factor of 3 below the value at which an excitation of bulk modes of the 3D crystalline beam is expected to occur. Their charac-
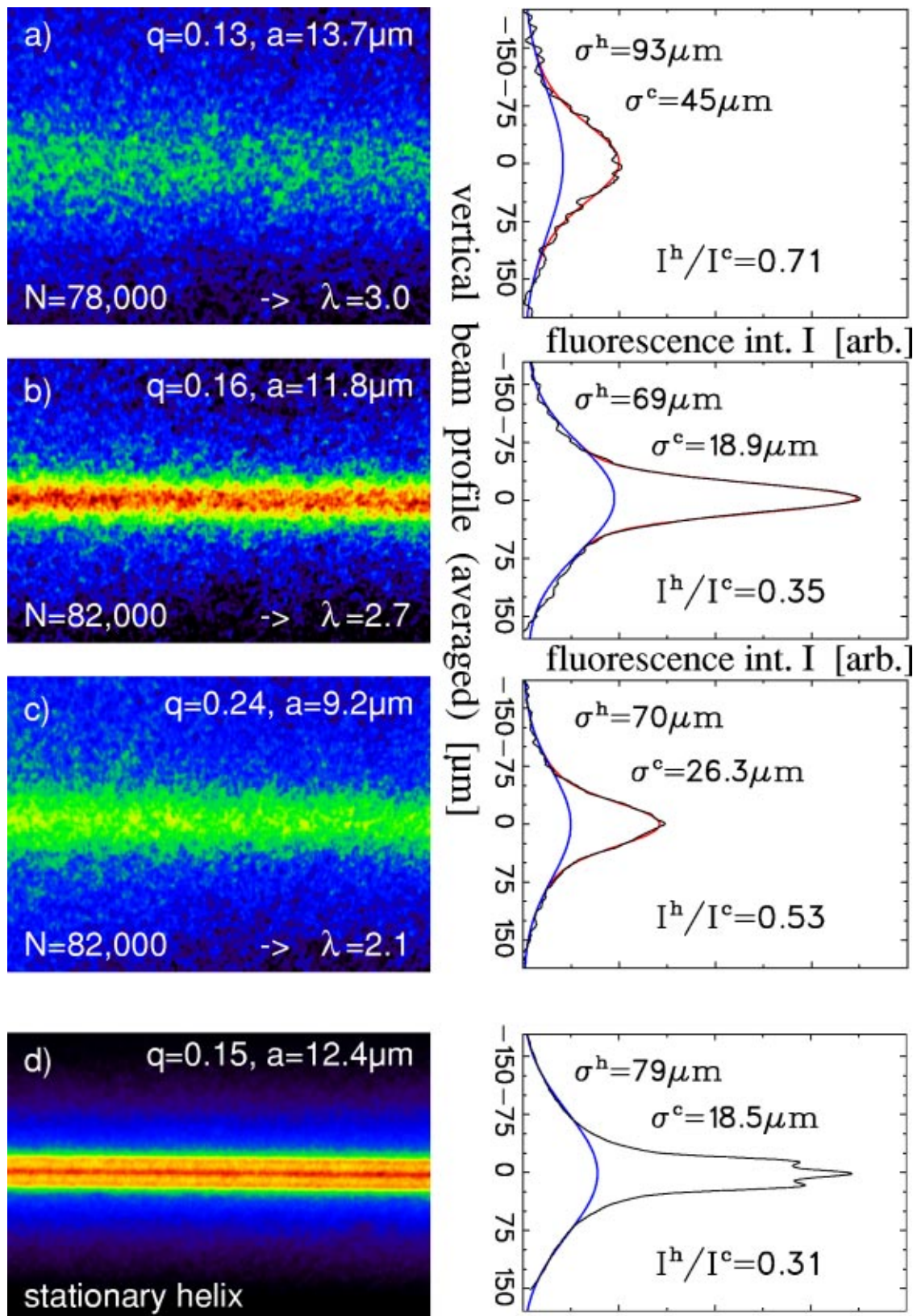
FIG. 4. (Color) Fluorescence image of an intense coasting ion beam ($N \approx 80\,000$). The vertical profile changes abruptly with rising confining potential from a broad noncrystalline beam (a) to a pronounced crystalline (b) and a slightly broadened one (c). Identical false-color coding is used from (a)–(c). As in Fig. 3, the blurred image of a long stationary helix is presented for comparison. The profiles are fitted as described in the caption of Fig. 3 and in Ref. [32].
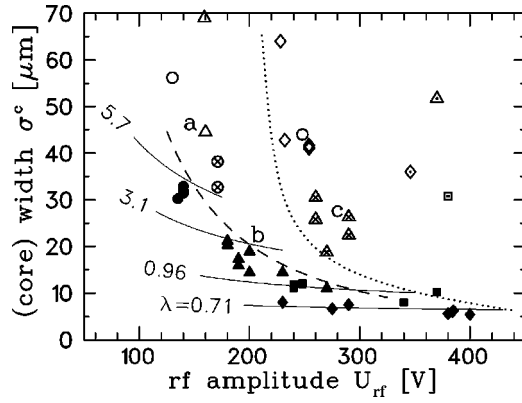
FIG. 5. Correlation of the absolute width of stored ion beams and the applied rf voltage. Crystalline beams are depicted as filled symbols, noncrystalline beams as open (focusing too weak), crossed, and dotted symbols (focusing too strong). The solid contour lines of constant linear density λ separate regions of different crystal structure, which is, in the following, expressed by the different symbols ($\blacklozenge$, strings; $\blacksquare$, zigzags; $\blacktriangle$, helix; $\bullet$, helix enclosing a string). The points labeled (a)–(c) correspond to the profiles shown in Fig. 4. The dotted line limits the region where stationary crystals could be observed in the storage ring PALLAS and in Ref. [8], the dashed line follows Eq. (1) as described in the text.

teristic frequency is close to the plasma frequency $\omega_p = \sqrt{2}\omega_{sec}$ [25]. To avoid an excitation of such bulk modes in the oscillating fields of the storage ring, the lowest possible sideband of the driving frequency $\Omega - \omega_p$ has to exceed twice the eigenfrequency ω_p or $\Omega > 2\omega_p$, which translates into the maintenance criterion $P > 2\sqrt{2}Q$ [11,12,34]. The importance of this rigid criterion was recently demonstrated in a dedicated linear ion trap [31]. This criterion is difficult to meet in existing heavy ion storage rings such as TSR (Heidelberg) with $Q = 2.8, P = 2$ [35] or ASTRID (Aarhus) [36], where the quest for crystalline beams has been of major interest. Although the secular frequencies in these heavy ion storage rings are almost equal to those in the storage ring PALLAS, the principle of rf focusing automatically fulfills the latter criterion, since $P/Q = 2\sqrt{2}/q$ with $q < 0.9$ for a sinusoidal drive.

The lower focusing limit in the λ-Q diagram appears to be rather constant for 3D beams but is considerably raised for the lower-dimensional crystalline beams. Below a certain focusing strength the ion density and thus the coupling between the transverse and the longitudinal degrees of freedom becomes too low to provide sufficient sympathetic transverse cooling. A transition to a broad but longitudinally cold beam occurs just before the beam is eventually lost. Here, at the limiting tune of $Q \simeq 45$ ($\omega_{sec} \simeq 2\pi \times 300$ kHz), the relaxation time ($2\pi/\omega_p$) amounts to about 1/3 of the transient interaction time with the laser beam. For $\lambda < 1$, the relaxation rate is further reduced since the number of neighboring ions is diminished and the border is shifted to stronger focusing. The absolute value of this lower border should strongly depend on the individual cooling scheme and especially on the amount of direct transverse cooling. Still, for $\lambda \gtrsim 1$, velocity dependent bending shear is expected to set limits, which can only be circumvented by cooling the beam
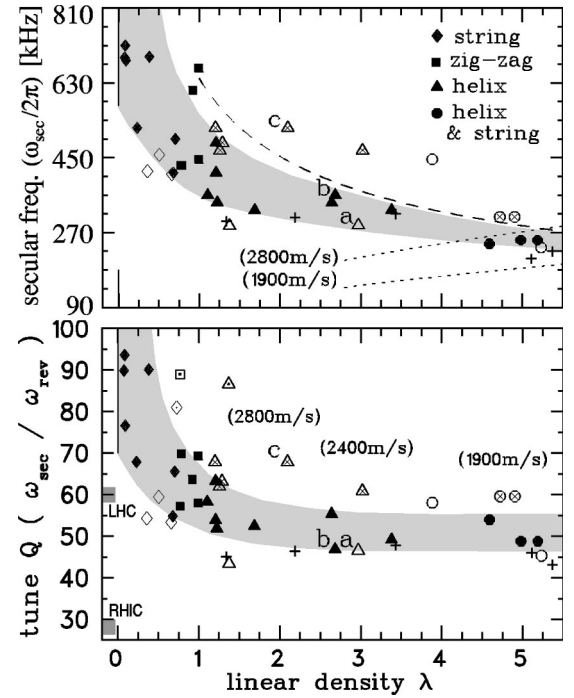

FIG. 6. Correlation of the linear density λ and the secular frequency of stored ion beams (upper frame). The shaded area marks the region where crystalline beams (filled symbols) were attained. The crosses ($+$) mark positions where beams were lost. The dashed line follows Eq. (1). At this line, the energy associated with the driven transverse oscillatory ion motion equalizes the melting temperature of the crystalline beam. The dotted line depicts the influence of bending shear, as given by Eq. (2). In the lower frame, where the focusing strength is characterized by the tune, the different beam velocities are indicated. Furthermore, typical tunes of the high-energy synchrotrons RHIC and LHC are given.

to constant angular velocity [11–13]. The dotted line in Fig. 6 shows an estimate [11] which stems from the relation of the mean centrifugal energy spread of the ordered beam to an apparent plasma parameter

$$\Gamma_{app}^s \approx 0.7 Q^2/\lambda. \quad (2)$$

This relation leads to a melting limit of $Q^2 \gtrsim 250\lambda$. When cooled to constant linear velocity, this energy spread is transferred into random motion. However, to a certain degree, an already existing crystal may withstand the bending due to its natural shear elasticity up to a limit of $Q \gtrsim \lambda$, as concluded from MD simulations [11]. The range of the present experiment comes close to these limits, and an anticipated increase of the beam velocity should allow stringent tests.

D. Beam profiles

In Fig. 7, the normalized width σ^c/a of crystalline and noncrystalline beams is presented as a function of the linear density λ. The dashed line shows the expected [7–9] dependence of σ^c/a of a crystalline beam on λ, which increases asymptotically as $\sigma^c/a \propto \sqrt{\lambda}$. For the convolution of the dashed curve with the experimental spatial resolution of the imaging system (≈ 4.5 μm) typical values of $a(\lambda)$ and thus
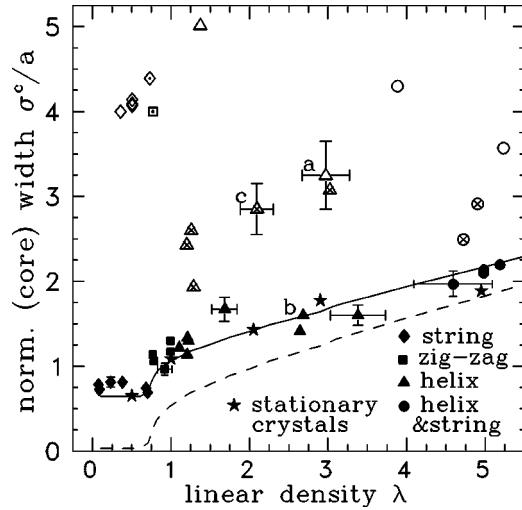
FIG. 7. Normalized width σ^c/a of various crystalline (filled symbols) and noncrystalline (open, crossed, and dotted symbols) ion beams and of stationary ion crystals (stars) as a function of the linear density λ. The points labeled (a)–(c) correspond to the beams shown in Fig. 4. Representative error bars are shown for the different states and sizes of the investigated ion beams.
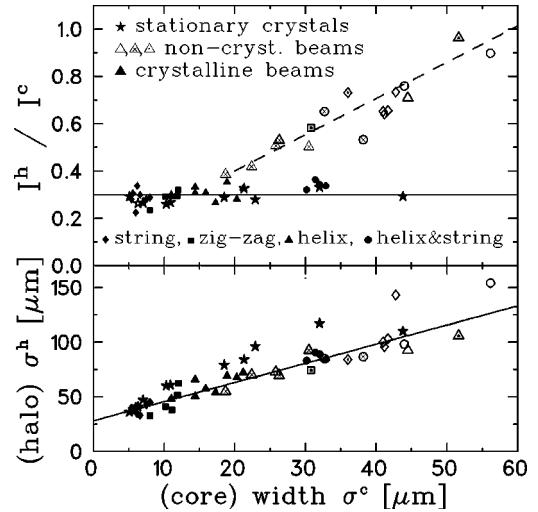

FIG. 8. Ratio of the fluorescence intensity of the two components of the bimodal vertical beam profile and width of the pedestal (halo) contribution of crystalline (noncrystalline) beams as a function of the width of the central (core) contribution.

of $U_{rf}(\lambda)$ have to be taken into account. As discussed with Fig. 5, the applied rf voltage has to decrease continuously with increasing λ to maintain the energy of the periodic transverse motion of the constituents of the crystalline beams below the melting threshold. Experimentally, the dependence $a(\lambda)$ is well determined. The resulting curve (solid line in Fig. 7) matches the behavior of the crystalline beams (filled symbols), which represent by far the narrowest beams, attainable for a given linear density. Their width, furthermore, coincides with that of stationary ion crystals (stars) recorded in the storage ring PALLAS under similar conditions. The abrupt reduction of the beam diameter, which was found to be characteristic for the phase transition, manifests itself in the wide gap that opens between the normalized width of the crystalline and those noncrystalline beams which were recorded at lower confining potential (open symbols). The fact that the particle number and thus the linear density is only known with an accuracy of at best 10% causes the slight and insignificant mismatch in the previous classification of the structure of the crystalline beams (compare Fig. 5) and the threshold values for λ in Fig. 7.

IV. HALO PROPERTIES OF NONCRYSTALLINE BEAMS

As mentioned in Figs. 3 and 4, the vertical beam profiles are characterized by a broad Gaussian pedestal and a central component of the beam with the widths σ^c and σ^h and the amplitudes I^c and I^h. In Fig. 8 the corresponding amplitude ratio I^h/I^c as well as the width of the pedestal σ^h are shown as a function of the central width σ^c. For crystalline beams as well as for stationary ion crystals we find a rather constant intensity ratio $I^h/I^c \simeq 0.3$. This consistency confirms the above interpretation of the Gaussian pedestal as an artifact [28]. Nevertheless, this experimental signature of a constant

ratio I^h/I^c might be useful for the identification of crystalline beams [5,6].

For the noncrystalline beams the ratio I^h/I^c increases with rising width σ^c. This unexpected behavior is interpreted as an increasing additional component of ions outside the dominant central region of the beam, a beam halo. The width of the halo σ^h increases linearly with σ^c, which indicates some correlation between both components. Notably, the beam still has a low velocity spread in the longitudinal direction. Yet, the fit of a bimodal Gaussian distribution to the comparatively weak fluorescence signals is connected with some ambiguity [32]. Interestingly, the beams that were focused too strong and thereby additionally heated (crossed symbols) show less halo than those that were focused too weak. For those beams, the coupling of the degrees of freedom is reduced, which possibly facilitates the formation of the beam halo. However, the reason for the formation of this distinct second component is unclear, and has not been observed in existing MD simulations concerning ion beam crystallization.

In the context of 1D crystalline beams, we recently speculated about the coexistence of short crystal fragments, which form the central core of the beam, longitudinally embedded in a halo of individual ions [5]. As both components have to maintain the average linear density, the observed correlation between the width of both components could be caused by their strong interaction. The fragments could be distributed over the circumference of the ring, based on the bistability of stationary ion clouds and crystals, which was observed in ion traps [20,21]. Yet, no underlying mechanism nor further experimental evidence has been found for this scenario at present.

V. CONCLUSIONS AND OUTLOOK

The ability to vary the focusing conditions of the storage ring PALLAS allowed the mapping of the range of

stability of crystalline ion beams in the λ-Q and λ-ω_{sec} planes up to a linear density of $\lambda = 5.5$. This range was found to be considerably reduced compared to stationary ion crystals and MD predictions. It seems that with increasing focusing strength the (weak) coupling of the unavoidable transverse periodic motion into thermal motion cannot be counteracted by the specific cooling conditions. Since no fundamental process is believed to hinder the beam crystallization, the demand for efficient cooling also in the crystalline regime has to be considered more carefully. The secular (betatron) frequencies and thus the absolute focusing strength of the storage ring PALLAS and typical heavy ion storage rings are comparable despite the great discrepancy in the (velocity dependent) periodicity and tune. With an anticipated increase in the beam velocity, the role of these parameters of focusing will be studied in the storage ring PALLAS in the near future as well as the influence of bending shear and the predicted necessity of cooling to constant angular velocity. For weaker focusing, direct cooling of the transverse degree of freedom is expected to extend the region of stability. Another way of approaching this difficult task in heavy ion storage rings [13,35] could be accomplished by means of a helical wiggler [16], which forces the ions onto a helical path. The wiggler provides a constant tilt angle between the ion and the cooling laser beam over a large dis-

tance. Part of the transverse ion velocity is projected in the longitudinal direction and can thus be directly addressed with a dedicated second cooling laser in a merged beam scenario.

In the long term, we anticipate the time resolved detection of fluorescence photons which are emitted by the individual ions, laser cooled to a constant beam velocity. The time correlation of this fluorescence signal contains information about the degree of crystallization of an ion beam. As it is expected for the case of the conventional Schottky noise of a circulating beam [37], this frequency analyzed *optical Schottky signal* should change from a broad peak at many harmonics of the revolution frequency into a sharp peak at N times the revolution frequency for a fully crystallized beam. A complementary approach could be the stroboscopic imaging of crystalline beams. This approach will be first tested for the case of bunched beams [5], where the bunching frequency is precisely known and facilitates the synchronization of the imaging system.

[1] J.P. Schiffer and P. Kienle, Z. Phys. A **321**, 181 (1985); A. Rahman and J.P. Schiffer, Phys. Rev. Lett. **57**, 1133 (1986).

[2] D. Habs and R. Grimm, Annu. Rev. Nucl. Part. Sci. **45**, 391 (1995), and references therein.

[3] *Crystalline Beams and Related Issues*, edited by D. M. Maletic and A. G. Ruggiero (World Scientific, Singapore, 1996).

[4] T. Schätz, U. Schramm, and D. Habs, Nature (London) **412**, 717 (2001).

[5] U. Schramm, T. Schätz, and D. Habs, Phys. Rev. Lett. **87**, 184801 (2001).

[6] U. Schramm, T. Schätz, and D. Habs, in *Non-Neutral Plasma Physics IV*, edited by F. Anderegg, C.F. Driscoll, and L. Schweikhard, AIP Conf. Proc. 606 (AIP, Melville, NY, 2001), p. 235.

[7] R.W. Hasse and J.P. Schiffer, Ann. Phys. (N.Y.) **203**, 419 (1990).

[8] G. Birkl, S. Kassner, and H. Walther, Nature (London) **357**, 310 (1992); I. Waki et al., Phys. Rev. Lett. **68**, 2007 (1992).

[9] M. Drewsen et al., Phys. Rev. Lett. **81**, 2878 (1998); L. Hornekaer et al., ibid. **86**, 1994 (2001).

[10] J. Wei, X.-P. Li, and A.M. Sessler, Phys. Rev. Lett. **73**, 3089 (1994).

[11] J. P. Schiffer, in *Crystalline Beams and Related Issues* (Ref. [3]), p. 217.

[12] J. Wei, et al. in *Crystalline Beams and Related Issues* (Ref. [3]), p. 229.

[13] J. Wei, H. Okamoto, and A.M. Sessler, Phys. Rev. Lett. **80**, 2606 (1998); H. Okamoto and J. Wei, Phys. Rev. E **58**, 3817 (1998).

[14] P. J. Bryant and K. Johnson, *Circular Accelerators and Storage Rings* (Cambridge University Press, Cambridge, UK, 1993).

[15] P. K. Gosh, *Ion Traps* (Clarendon Press, Oxford, 1995).

[16] U. Schramm, Habilitation thesis, LMU Munich, Universität Munchen, 2001 (unpublished); T. Schätz, U. Schramm, and D. Habs, in Crystalline Ion Beams, edited by A. Noda (unpublished).

[17] H. J. Metcalf and P. van der Straten, *Laser Cooling and Trapping of Atoms and Ions* (Springer-Verlag, Berlin, 1999).

[18] H.-J. Miesner et al., Phys. Rev. Lett. **77**, 623 (1996).

[19] The two laser beams had to be tilted by an angle $\alpha \approx 0.5$ mrad with respect to each other in the horizontal plane to avoid perturbing effects between the two independently stabilized laser systems. Such an adjustment automatically leads to a tilt angle $\alpha^* \leq \alpha$ with respect to the ion beam.

[20] F. Diedrich, et al., Phys. Rev. Lett. **59**, 2931 (1987).

[21] R. Blümel et al., Nature (London) **334**, 309 (1988); Phys. Rev. A **40**, 808 (1989).

[22] Systematic studies of the formation of large prolate ion crystals in a linear Paul trap [9], as a function of the laser detuning, confirmed this interpretation of the dip in the range of few cylindrical shells, as reported in L. Hornekaer, Ph. D. thesis, University of Aarhus, Denmark, 2000 (unpublished).

[23] For the calibration of the fluorescence yield per ion in a crystalline beam, the absolute number of ions in a stationary ion crystal was directly counted. These ions were accelerated and the corresponding fluorescence rate was measured in flight and at rest.

[24] D.H.E. Dubin, Phys. Rev. A **42**, 4972 (1990).

[25] D.H.E. Dubin, Phys. Rev. E **53**, 5268 (1996); D.H.E. Dubin

and J.P. Schiffer, *ibid.* **53**, 5249 (1996).

[26] J.P. Schiffer, Phys. Rev. Lett. **88**, 205003 (2002).

[27] For crystalline beams, a larger relative detuning of the two laser beams in the ion rest frame had to be chosen than in the case of stationary ion crystals [29]. This fact might be due to the increased sensitivity of the crystalline beam to the mechanism of diffusive transverse heating which is associated with the random scattering of laser photons. As a consequence, the fluorescence signal was lower by about a factor of 5.

[28] A similar pedestal occurred in the original investigation of stationary ion crystals performed by Walther and co-workers [8] in their rf quadrupole ring trap, which has the same dimensions and used a similar optical imaging system as the storage ring PALLAS (see [5,6]). Furthermore, the appearance of the pedestal in the images of stationary ion crystals (where single ions are resolved) and crystalline beams support the interpretation as an artifact. As light scattering in the optical imaging system seems to be its origin, the parameters of the Gaussian pedestal (σ^h, I^h) depend on the shape and the brightness of the original object.

[29] T. Schätz, U. Schramm, and D. Habs, in Atomic Physics at Accelerators III, Aarhus, Denmark, edited by J. Hangst [Hyperfine Interact. (to be published)].

[30] Q. Spreiter, M. Seurer, and C. Toepffer, Nucl. Instrum. Methods Phys. Res. A **364**, 239 (1995); M. Seurer, Q. Spreiter, and C. Töpffer, Hyperfine Interact. **99**, 253 (1996); in *Crystalline Beams and Related Issues* (Ref. [3]), p. 311.

[31] N. Kjaergard, K. Molhave, and M. Drewsen, in *Non-Neutral Plasma Physics IV* (Ref. [6]), p. 145.

[32] For *crystalline beams* the width σ^c can be determined with a relative error of about 5%, as the Gaussian pedestal (in this case an artifact [28]) can be unambiguously distinguished. Representative error bars are given in Fig. 7. The relative error of the amplitudes amounts to about 5% for I^c and 10% for I^h. For *noncrystalline beams*, where the separation of the two components becomes more ambiguous, the relative error in the width increases to about 10–15 %. A larger uncertainty shows up in the determination of the amplitudes ($\approx 30\%$ for I^h and $\approx 10\%$ for I^c).

[33] J.P. Schiffer *et al.*, Proc. Natl. Acad. Sci. U.S.A. **97**, 10 697 (2000).

[34] T. Kihara *et al.*, Phys. Rev. E **59**, 3594 (1999).

[35] U. Eisenbarth *et al.*, Hyperfine Interact. **127**, 223 (2000); I. Lauer, *et al.*, Phys. Rev. Lett. **81**, 2052 (1998); and references therein.

[36] N. Madsen *et al.*, Phys. Rev. Lett. **87**, 274801 (2001), and references therein.

[37] V.V. Avilov and I. Hofmann, Phys. Rev. E **47**, 2019 (1993).